Advanced Fabrication, Modeling, and Testing of a Microphotosynthetic Electrochemical Cell for Energy Harvesting Applications

Arvind Vyas Ramanan, *Student Member, IEEE*, Muthukumaran Pakirisamy, *Member, IEEE*, and Sheldon S. Williamson, *Senior Member, IEEE*

***Abstract*—Unconventional renewable energy sources are scarce and have not been explored thoroughly or exploited. The photosynthetic power cell (PSC) is one among them. Though there are few prototypes fabricated earlier, there has not been a comprehensive electrical equivalent model developed. This paper proposes an electrical equivalent model for a microphotosynthetic power cell (μPSC), which is tested and authenticated with experimental verification on a fabricated prototype. The developed model is further used for testing emulation behavior, to efficiently and accurately design an energy harvesting power electronic converter. The principle of the operation of the device is based on "photosynthesis." Photosynthesis and respiration both involve an electron transfer chain. The electrons are extracted with the help of electrodes and a redox agent, and a power electronic converter is designed to harvest the energy. The fabricated cell is capable of producing an open-circuit voltage of 0.9 V and about 200 μW of peak power. The μPSC has an active area of $4.84\,\mathrm{cm}^2$, which approximately translates to a power density of $400\,\mathrm{mW/m}^2$. This makes it as one of the best-performing μPSC. The other top-performing μPSC devices report power densities of between 100 and $250\,\mathrm{mW/m}^2$. The PSC produces energy under both dark and light conditions.**

***Index Terms*—Photosynthesis, photosynthetic power cell (PSC), power electronic converter, renewable energy.**

I. Introduction

THE need for energy is inevitable for mankind. Climate change, depletion of natural resources, pollution, and other factors have created the necessity to look for energy from renewable sources. Furthermore, there are challenges aplenty in the field of renewable energy as renewable energy sources are unpredictable, nondependable, and limited, such as wind, solar, and tidal power. Apart from these, there are few unconventional renewable energy sources that have not been explored thoroughly or exploited. The photosynthetic power cell (PSC) is one among them.

The PSC harvests the energy produced at the lowest level of the food cycle "photosynthesis" in plants. The PSC extracts the energy produced during photosynthesis and respiration in form of electrical energy [1]. The developed device differs from other published works [1], [2] in terms of improved performance, fabrication technique, and material of structure. The two main types of sources used in the PSC are aerobic unicellular organisms (e.g., algae and cyanobacteria) and subcellular thylakoid photosystems/chloroplasts isolated from plant cells (e.g., spinach plant's subcellular thylakoid photosystems isolated from the plant cells) [3]. The PSC produces energy under both dark and light conditions.

The developed PSC is a polymer-based structure instead of silicon, integrating the conventional MEMS processes with polymers. The principle of the operation of the device is based on "photosynthesis." Photosynthesis and respiration both involve an electron transfer chain. The electrons are extracted with the help of electrodes and a redox agent (potassium ferricyanide), and a power electronic converter is designed to harvest the energy [2]. The developed device is capable of producing an open-circuit voltage (OCV) of 0.9 V and about 200 μW of peak power. The μPSC has an active area of $4.84\,\mathrm{cm}^2$, which approximately translates to a power density of $400\,\mathrm{mW/m}^2$. This makes it as one of the best performing μPSC. The other top-performing μPSC devices report power densities between 100 and $250\,\mathrm{mW/m}^2$ [3]. The device working principle, testing, and experimental results of developed cell, electrical equivalent circuit modeling, and simulation with a power electronic converter are discussed in detail in the following sections.

This paper is organized as follows. In Section II, the PSC device is explained. Section III identifies the important operation parameters, experimental procedure, and results. Section IV presents the modeling approach, electrical equivalent model, and the simulation model results and compares them with the experimental results. Section V draws out the conclusion.

II. Device Principle and Operational Characteristics

The microphotosynthetic power cell (μPSC) converts energy from sunlight to electrical energy through the biochemical processes occurring in different microorganisms and by inducing redox reactions. The PSC unlike solar can produce power during dark period as well, and unlike the fuel cells it replenishes

Manuscript received February 1, 2013; revised May 8, 2013 and August 5, 2013; accepted September 5, 2013. Date of publication April 15, 2014; date of current version October 15, 2014. Recommended for publication by Associate Editor C. Fernandez.

A. V. Ramanan and S. S. Williamson are with the Power Electronics and Energy Research (PEER) Group, P. D. Ziogas Power Electronics Laboratory, Department of Electrical and Computer Engineering, Concordia University, Montreal, QC H3G 1M8 Canada (e-mail: vyas555@gmail.com; sheldon@ece.concordia.ca).

M. Pakirisamy is with the Department of Mechanical and Industrial Engineering, Concordia University, Montreal, QC H3G 1M8, Canada (e-mail: pmuthu@alcor.concordia.ca).

Color versions of one or more of the figures in this paper are available online at http://ieeexplore.ieee.org.

Digital Object Identifier 10.1109/TPEL.2014.2317675

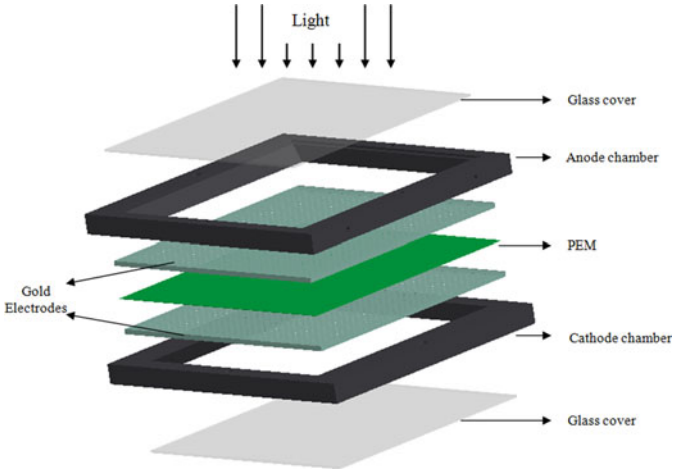

Fig. 1. μPSC schematic assembly.

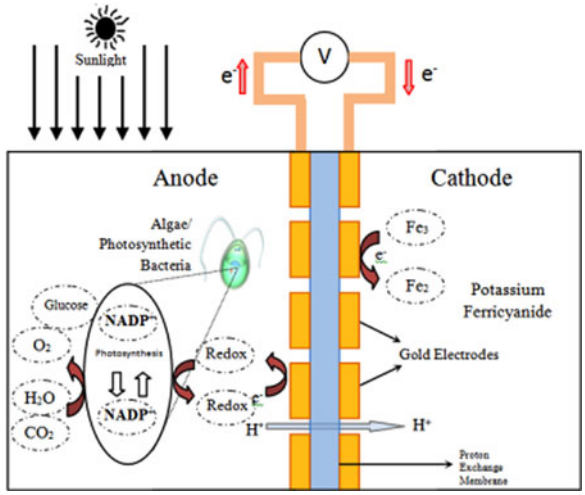

Fig. 2. μPSC—principle of operation.

itself without having to supply additional fuel when energy is consumed. The operation of the device is based on the electron transfer that occurs during photosynthesis and respiration, which are the same reactions when reversed. Thus, it makes the PSC functional during light and dark and is self-restoring. The following are the chemical reactions that occur during photosynthesis and respiration [1]:

$$\text{Photosynthesis (light)}: CO_2 + H_2O \rightarrow (CH_2O) + O_2 \quad (1)$$

$$\text{Respiration (dark)}: (CH_2O) + O_2 \rightarrow CO_2 + H_2O. \quad (2)$$

Both photosynthesis and respiration involve electron transfer chains, from which a free electron can be extracted. In μPSC, these electrons are extracted with the help of redox reactions and are passed through an external electrical circuit, which gives rise to the electric current.

A. Device Construction

The μPEC is similar in construction to that of an electrochemical cell like the fuel cell. The device consists of two identical half-cells, each forming the anode and the cathode separated by a proton exchange membrane (PEM), which is a sulfonated copolymer, usually Nafion. The anode and the cathode sides are sealed with glass on top to allow light to pass through for photosynthesis. A porous gold electrode is fabricated on top of both the surfaces of the PEM, which acts as the current collector. The PEM allows only the positive ions to the cathode side and blocks the electrons. The gold electrode helps in trapping the free electrons. The gold electrodes are connected to an external circuit, and the passing electrons produce the electric current. This is analogous to most of the electrochemical cells. The free electrons are derived from the electron transfer that occurs during photosynthesis and respiration. Thus, it makes the PSC functional during light and dark and is self-restoring. The schematic assembly of the device is shown in Fig. 1.

The anode chamber is filled with the algal/bacterial medium (anolyte) and cathode chamber with the potassium ferricyanide (catholyte). Thin gold sputtered aluminum strips are attached to the electrodes anode and cathode, to which any external electrical connection can be made. The fabrication of these main components is of a major difference between this paper and earlier PSCs. The fabrication process will be discussed in details in the following chapter where each component is explained separately. One of the main differences to be mentioned is that unlike in the previous works, which were silicon-based devices [5].

B. Device Operating Principle

PSCs generate electricity from both photosynthesis and catabolism of endogenous carbohydrates in the light and from catabolism alone in the dark. The PSC operating principle is illustrated in Fig. 2, which shows the anode and cathode reaction chambers separated by a PEM and are connected to an external circuit through electrodes.

In the anode chamber, a live culture of algae or a photosynthetic bacterium such as the cyanobacteria is suspended in a growth media solution with a redox coupler or an electron mediator. During the presence of light, photosynthesis takes place in the microorganisms. The microorganisms convert CO_2 and H_2O into O_2 and carbohydrates (e.g., glucose). During photosynthesis, electrons are transferred by diffusion of electron carriers NADPH or along a electron chain carried out in the series of thylakoid-bound enzyme complexes called the photosystems. These electrons (and protons) are siphoned from the normal photosynthetic process either from NADPH or from the transport chain by redox coupler/electron mediator molecules that have diffused into the microorganisms. The reduced (electrons and protons carrying) compounds diffuse out of the microorganism's cell, through the mediator solution; the electrons close to the anode are attracted by the redox potential of the catholyte. Due to this potential, the electrons then travel through the connected external load into the cathode chamber, similar to a MFC. At the cathode, they reduce the oxidant ferricyanide (Fe_3). Meanwhile, the protons (H^+) at the anode diffuse across the PEM from the anode into the cathode, where they reduce

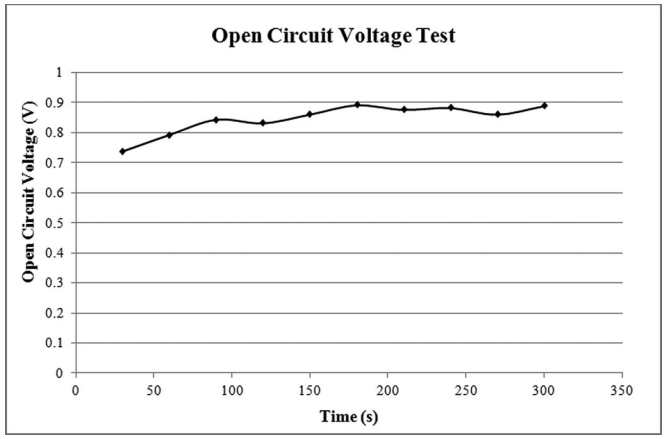

Fig. 3. OCV testing.

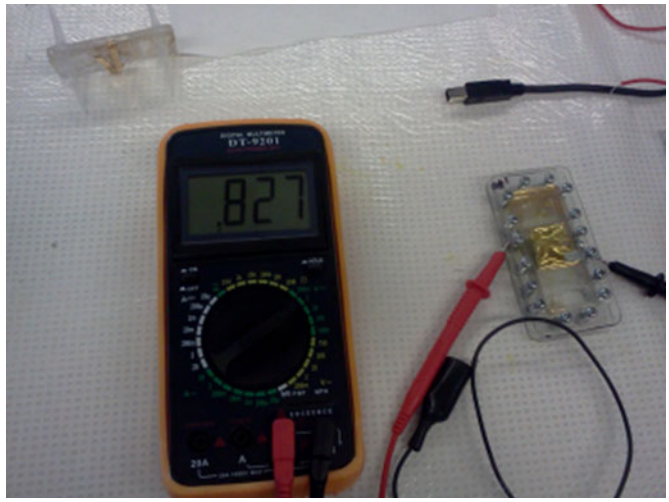

Fig. 4. OCV testing of the assembled device.

the oxidant (Fe_2) or combine with O_2 and electrons from the reduced oxidant to release H_2O [1], [2], [5].

III. Experimental Setup, Test Results, and Critical Parameters

The individual cell components are assembled, and the necessary reactants/solutions are prepared. A 25% (w/w) potassium ferricyanide $(K_3[Fe(CN)_6])$ solution is prepared and is used as the catholyte. A volume of 2.0 mL of the prepared catholyte is pumped in to the cathode chamber through the channels with caution. A well-assembled device has no leaks. The anode chamber is then filled with 2.0 mL of the anolyte solution, containing the green algae (*Chlamydomonas reinhardtii*), the growth medium, and other reactants. Once the set up is ready, different experiments are performed to observe cell performance. However, it should be tested first. For testing the cell, a simple OCV test is performed. All the tests were performed under ambient room condition of light and temperature.

A. OCV Testing

An OCV observation is one of the best ways to test a newly developed or fabricated electrical cell. A quick inference can be drawn from the open circuit that a cell produces. Cells that are assembled poorly, or are made up poorly fabricated components, produce very low, or nearly zero voltage. If the device has leaks, the initial OCV produced will be good. However, this rapidly reduces to zero. A well fabricated cell produces a steady OCV of 0.6–1.0 V (depending on various parameters). Thus, when a device is fabricated and assembled, the cell OCV performance is initially observed, to check the device quality. A sample OCV test result is shown in Fig. 3. The OCV test setup is shown in Fig. 4. The voltage of the cell is observed for about 5 min, without any load (OCV).

B. Load Testing

The load test is performed to observe, if the cell is capable of producing power. A load of 1 kΩ is connected with to the cell, and the now, the voltage and current are measured and observed for the same period of time. The cell voltage and current under a load of 1.0 kΩ is shown in Fig. 5. Also, the cell takes some time to respond to switching, as shown in Fig. 6.

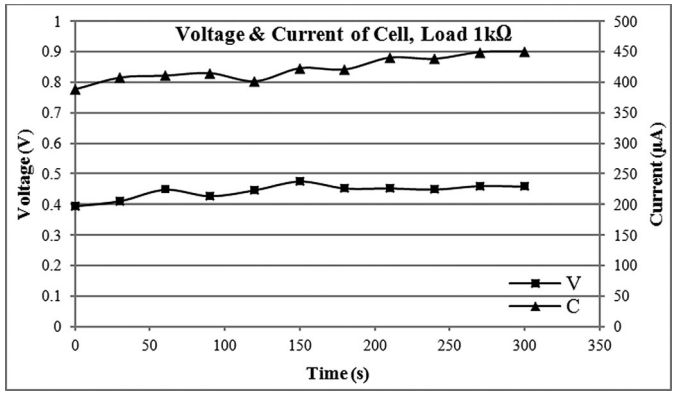

Fig. 5 Cell voltage (in volts) and cell current (in microamperes) under a load of 1 kΩ.

It can be clearly seenthat the cell is in good condition and is able to produce power continuously.

C. V/I and Power Characteristics of μPSC

Voltage–current (V/I) characteristics are studied to determine the basic parameters and are used to model its behavior in an electrical circuit of any electrical or electronic device. The V/I characteristics are obtained linearly varying the load on the cell. The cell was initially loaded at approximately at 1 Ω and was increased gradually up to 10 MΩ. The following graph illustrates the V/I characteristics obtained for one of the cells. The tests were conducted under ambient temperature and lighting conditions.

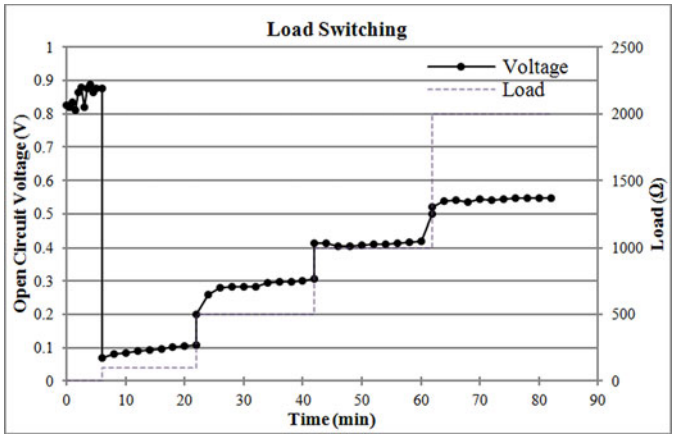

Fig. 6. Load switching response of the fabricated cell.

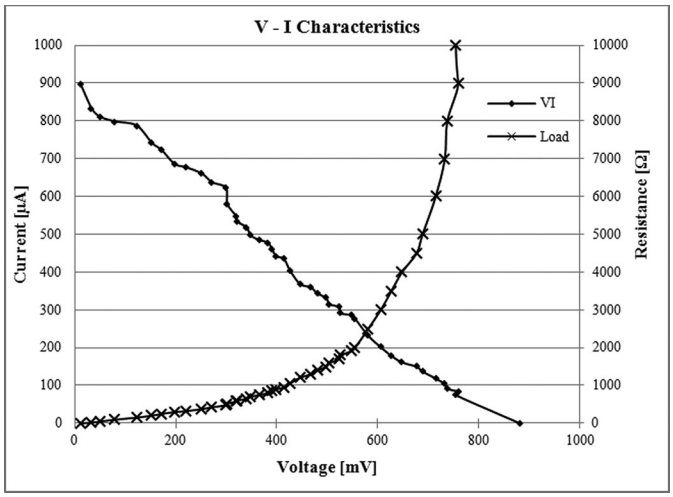

Fig. 7. V/I characteristic of the cell.

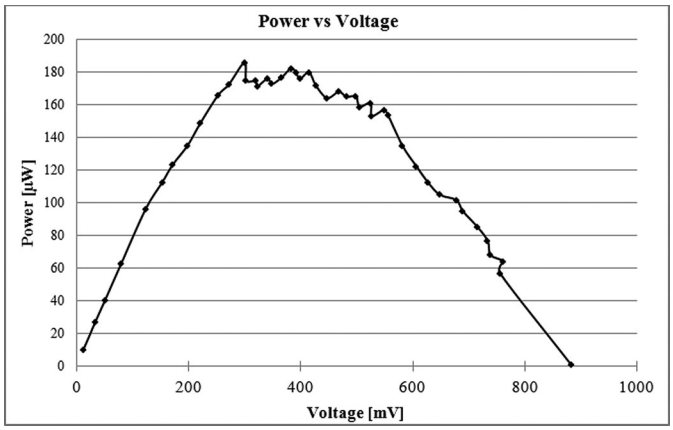

Fig. 8. Power characteristic of the cell.

The cell generates a peak power of about 190 μW, as is clear from Fig. 8. From the V/I plot of Fig. 7 as well as the power plot of Fig. 8, it can be logically inferred that the preferable working range for PSC would be from 300 to 600 mV. The peak power of 190 μW of the cell corresponds to $39.25\,\mu\mathrm{W/cm^2}$, since the area of one cell is 2.2 cm $\times$ 2.2 cm. These characteristics can be used to achieve the maximum power point (MPP) of the cell.

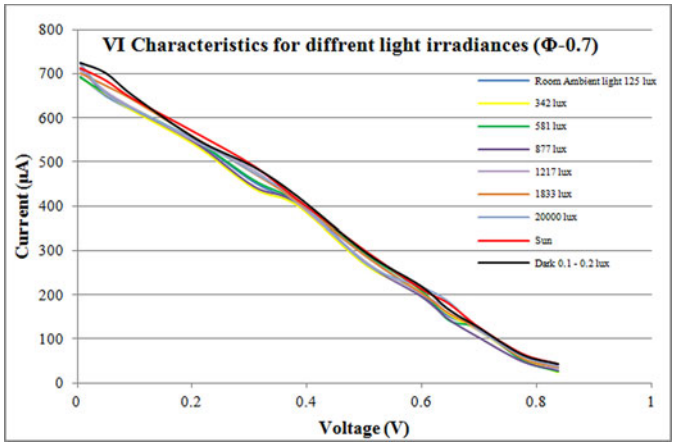

Fig. 9. V/I characteristics for different light irradiances.

From the earlier discussions, it is clear that the fabricated device has been successfully tested and that the electrical performance characteristics (voltage, current, and power) are satisfactorily obtained. The next step is to examine the various parameters affecting the cell's performance and electrical characteristics.

D. Parameters Affecting Cell Performance

Three main environmental factors, light irradiance, temperature, and carbon dioxide concentration, influence the photosynthetic activity entirely.

1) Effect of Light Irradiance: The rate of photosynthesis depends on the irradiance of light (illuminance in photometry). During complete dark period (no light), plants respirate. It should be noted that the photosynthesis rate saturates around $165\,\mathrm{W/m^2}$ (41.085 lx) for algae or organisms with chlorophyll as the main photosynthetic pigments.

For these tests, a closed opaque cardboard chamber was made and was fitted with four 60-W incandescent bulbs. Along with it was placed the lux-meter, to measure the light irradiance. There was no ambient light entering the chamber. When there were no bulbs on, it was completely dark inside the chamber, and each light was turned on one-by-one, to increase the light intensity and observe its effects. Apart from performing the tests inside the chamber, the same test was done in ambient light in the lab and also directly in sunlight (was placed directly under sunlight, near a window). The V/I and power characterization of the cell was then performed. Nafion 115 was used as the PEM for all of the experiments and the quantum yield of the cells used were 0.7 (refer page 12 page 3 for quantum yield definition). The plots in Figs. 9 and 10 show the V/I and power characterization of the cell under different lighting conditions.

The minimum light irradiance $\left(\mathrm{E/cm^2 \cdot s}\right)$ for maximum photosynthetic activity depends on the wavelength of the incident light and is usually of the order of 50–100 $\mathrm{nE/cm^2 \cdot s}$ [7]. The photosynthetic activity is a measure based on the amount of carbon dioxide absorbed per unit area per second. The

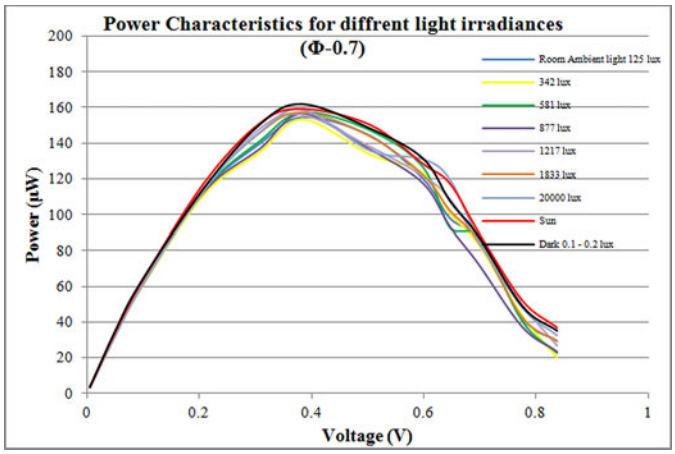

Fig. 10. Power characteristics for different light irradiances.

TABLE I
DESCRIPTION OF PARAMETERS FOR DERIVATION OF ENERGY CONTAINED IN A PHOTON

Symbol	Quantity	Unit/Conversion from CGS to SI
E	Einstein (light irradiance)	1mol of photons →6.022 x 10^{23} photons
h	Plank's Constant	6.626068 × 10^{-34} m^2 kg / s
c	The speed of light	299,792,458 m / s
λ	Wavelength of light	m
n	nano	10^9

photosynthetic activity of common chlorophyll based plants usually saturates around 85–100 $\mathrm{nE/cm^2 \cdot s}$ [8].

The energy of a photon is given by the equation

$$\text{Energy} = \frac{hc}{\lambda}. \tag{3}$$

Table I gives the details of each parameter used in the derivation of (3).

Green plants usually absorb the light close to red and blue spectrum. The wavelength of red light is higher than that of blue light. On conversion of units, power per unit area of blue light is around $165\,\mathrm{W/m^2}$. The figure below shows the visible light spectrum and absorbance of wavelength of chlorophylls [8]. It can be observed that there is not much difference in the power produced at different light irradiances. The cell produces slightly more power in the dark compared to maximum light condition under the sun; this is because during respiration/dark periods, the cell behaves like a microbial fuel cell (MFC).

It can be observed from Fig. 10 that there exists not much difference in the power produced at different light irradiances. The cell produces slightly more power in the dark compared to maximum light condition under the sun. This is because, during respiration, the cell behaves like an MFC.

2) Nafion Thickness: The Nafion PEM is available in different thicknesses. Thicker the Nafion, more robust it is; thicker Nafion depicts higher electron resistance. Two membranes, Nafion 115 and Nafion 117, were tested, as the results shown in Figs. 11 and 12 were quite conclusive.

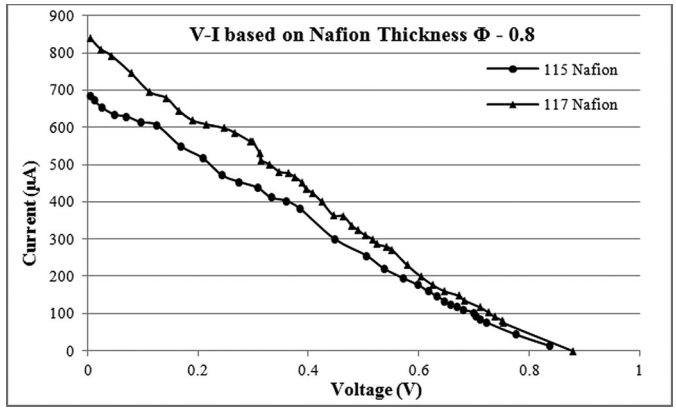

Fig. 11 V/I characteristics for different Nafion membranes.

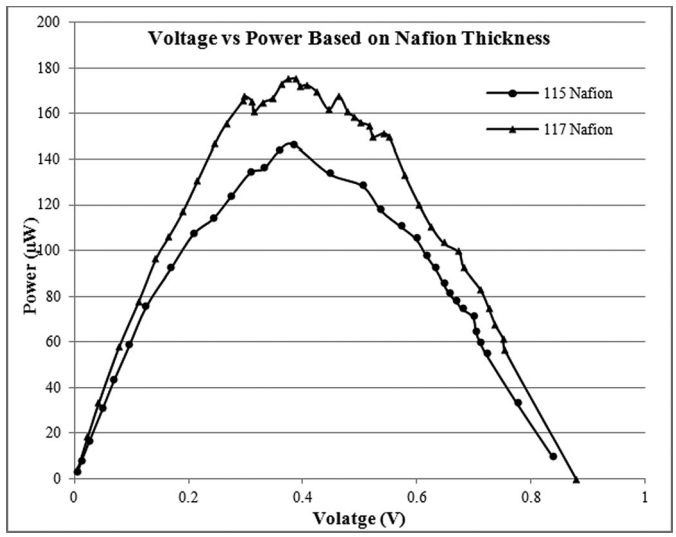

Fig. 12. Power characteristics for different Nafion membranes.

All parameters were the same for both the tests; the only difference was the different type of Nafion used. The cell produces more power and voltage, when a thicker PEM membrane is used. This is caused because the thicker membrane has higher resistance toward the electrons, and therefore, more electrons are made to travel through the external circuit, instead of passing through the membrane (leakage current). This increased resistance causes the increase in power, compared to the thinner Nafion.

3) Quantum Yield: Since the goal of the device to produce maximum power, it is assumed that the best PEM will always be used as well as the minimum light irradiance of 41 lx is easily present. Thus, it is not necessary to model the cell based on the two parameters mentioned earlier. However, the tests mentioned earlier did not give consistent results in the beginning, even on using the same PEM, same lighting conditions, algae concentration, and other physical parameters. On further investigation, the most important factor was determined to be the quantum yield (Φ) of photosystem of algae. For the tests performed initially, though the same concentration of algae samples were used, they did not have the same quantum yield and thus led to different voltages and power levels. On using the algae with same

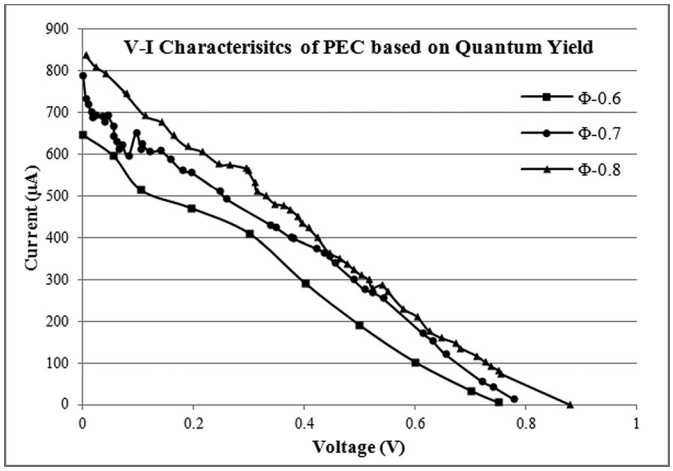

Fig. 13. V/I characteristics for different quantum yield samples.

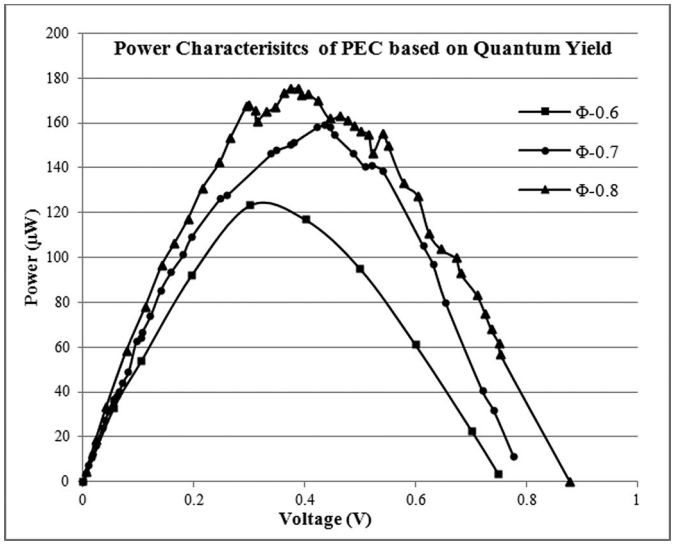

Fig. 14. Power characteristics for different quantum yield samples.

quantum yield it was observed that the test provided consistent results.

Quantum yield (Φ) is defined as the number of molecules or electrons given out per photon absorbed by the system. It will be easier to understand the quantum yield Φ with an example of fluorescence, where it is the number of photons emitted to that of photons absorbed [6]

$$\Phi = \frac{\text{number of molecules affected}}{\text{total number of photons absorbed}}. \tag{4}$$

In a photochemical process, when a molecule changes state, after absorbing a light quantum (photon), the quantum yield is the ratio of number of changed molecules to the number of photons absorbed. Since it is not possible to absorb all the photons efficiently, quantum yield will always be less than 1.0. The value of Φ for a particular process can range from 0 to 1.0. Quantum yield of a process is 0 when the involved molecule or particle does not change its state of excitation, and it is 1.0 when the process is excited with the same level of energy. Quantum yield (Φ) of the algae (*C. reinhardtii*) samples of used ranged from 0.5 to 0.8. It was observed that higher the quantum yield, higher the power output of the cell. Presented in the plots in Figs. 13 and 14 are the experimental test results, where V/I and power characteristics are observed for different quantum yields. The tests were conducted with *C. reinhardtii*, with a quantum yield of $0.589 \approx 0.6$; $0.712 \approx 0.7$; $0.796 \approx 0.8$, respectively. Other parameters for the tests remained same and were performed in ambient light and temperature conditions.

It can be clearly observed from Figs. 13 and 14 that the quantum yield of the samples significantly changes the characteristics of the cell. The cell with a quantum yield $\Phi = 0.6$ produces approximately a peak power of 125 μW, $\Phi = 0.7$ produces a peak power of around 150 μW, while $\Phi = 0.8$ produces around 180 μW peak power. Furthermore, the OCV produced by the cells is also different, when quantum yield varies, as is evident from Fig. 13.

4) Temperature Variation: The effect of temperature on photosynthesis is a very important consideration. It is worth mentioning here that the light-dependent reactions are not affected by changes in temperature. The light-independent reactions are reactions catalyzed by enzymes. The light-independent reactions of photosynthesis are indeed dependent on temperature [9]. As the temperature increases, the enzymes approach their optimum temperature of operation, and the overall rate increases. The rate of increase approximately doubles for an increase of temperature by 10 °C. Once the temperature continues to rise beyond the optimum temperature, the rate begins to decrease rapidly, until it comes to a halt, since the enzymes are denatured [10], [11]. The cell would mostly be operating under these conditions and need not be considered as a major parameter affecting the performance of the cell.

IV. Modeling of the Photosynthetic Cell (PSC)

Experimental based model verification is the obvious method of choice to validate the cell. Experimental-based modeling or curve fitting is the process of formulating a mathematical function (polynomial equation/curve) that fits best to all the data points with the least deviation. For the interpolation to be smooth between the data points, a smooth function can be constructed for an almost exact fit to the data. Fitting the curve outside the range of the observed data is called extrapolation and has a greater degree of uncertainty, as it would use the same method to relate the available data.

To develop a model for the fabricated cell, data from different experimental results are curve fitted and the relationship between the parameters is understood. These functions for different relationships are surface fitted (when more than two parameters are curve fitted, it is referred to as surface fitting), and the final interrelational function (or a lookup table) is obtained. Using the "Basic Fitting" tool in MATLAB, data for the V/I characteristics for different quantum yield of the cells are curve fitted and the function is derived. The curve-fitting equations are as follows:

$$I = -V \times 0.861 \times 10^{-3} + 0.636 \times 10^{-3}\,(A), \quad \text{for } \Phi = 0.6 \tag{5}$$

$$I = -V \times 0.881 \times 10^{-3} + 0.719 \times 10^{-3}\,(A), \quad \text{for } \Phi = 0.7 \tag{6}$$

$$I = -V \times 1.003 \times 10^{-3} + 0.827 \times 10^{-3}\,(A), \quad \text{for } \Phi = 0.8. \tag{7}$$

It can be seen that the constant term in (5), (6), and (7) are approximately equal to the quantum yield multiplied with a factor of 10^{-3}. Also, the change in the short circuit current and OCV is substantial with the quantum yield of the cell changing. There exist a few mathematical models that have been proposed for MFCs [12]–[15]. These models include the electrochemical model, biochemical model, biofilm model, and the bulk liquid model, to name a few. Most of these models are based on Nernst equations; the structure and parameters of the models are complicated, also the process of modeling is complex. A basic simple model, which can provide important and accurate predictions of the cell operating conditions so that the model can be used in simulations and be used for optimization of the performance of MFC, is more applicable. Therefore, establishing a simple model for the μPSC was given all the attention. In order to obtain the operating point precisely based on the factors, it is necessary to have a surface fit from the fitted curves. The surface fit function represents a three dimensional surface, which corresponds to an operating point based on three different parameters. Surface fitting of equations based on Nafion thickness are not necessary because the best thickness can be chosen when fabricating the device and will remain constant. Also, surface fitting of equations based on light irradiance does not seem necessary as all the equations can be approximated to single equation with the error between the functions being negligible. The curve fitting equations obtained for experiments based on quantum yield of the cell ((5) to (7)) were used for developing the surface fitting function. The surface fit function is of the form $z\,(x, y)$. The cell current is represented by the z-axis, the cell voltage as x-axis, and the quantum yield as y-axis. Thus, the cell current is represented by the cell voltage and quantum yield of the cell. The published work of Markvart and Landsberg [16] shows that that the primary photosynthetic reaction closely resembles the operation of a solar cell. The photosynthetic reaction rate and process can be represented in a form similar to the Shockley solar cell equation. The photosynthetic reaction produces both chemical and electrical energy (from the electron transfer chain). Energy divided into these two components is predictable, and makes it possible to optimize the amount of power produced. Thus, the MPP of the photosynthetic organism can be tracked. This can used to estimate the maximum energy that can be produced as well as compute the various losses [16].

The electron transport chain occurs in the photosynthetic reaction center, which is a protein complex binding component of the electron transport chain. The primary electron donor is a chlorophyll molecule (B), pheophytin (H), and a quinone (Q). Electron is excited by light from the ground state of P to an excited state P^* (transferred successively from B, H, and, finally, Q). An electron replenishes the ground state of the primary donor, and the electron transfer cycle starts again [16]. A simplified schematic diagram for the model with the notations is shown in Fig. 15.

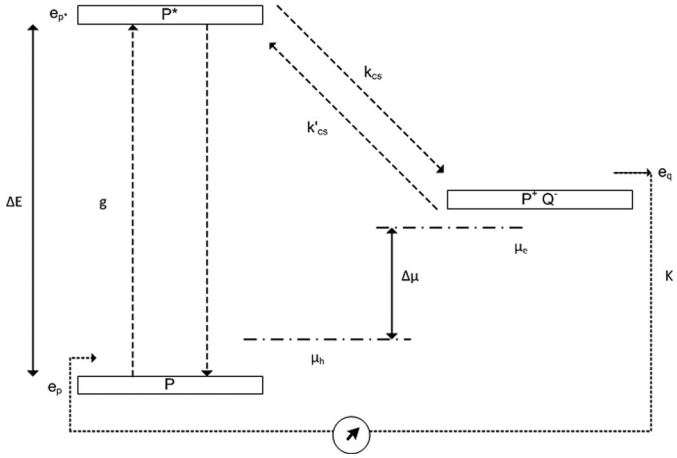

Fig. 15. Schematic model of electron transport during photosynthesis.

Here:

1) $1/\tau$ is the lifetime of the electron in the excited state P^*;
2) g is the photo-excitation rate of P;
3) K is the rate of electron removal from the photosynthetic reaction centre at Q (it's the actual rate of the photosynthetic energy conversion);
4) $\Delta\mu$ is the maximum energy generated per electron;
5) k_{cs} is the rate constant for charge separation from $P^* \rightarrow Q$;
6) k'_{cs} is the rate constant for the reverse process.

The rate constants k_{cs} and k'_{cs} satisfy the detailed balance criteria:

$$\frac{k'_{cs}}{k_{cs}} = \exp\left(\frac{e_q - e_p^*}{k_b T}\right). \tag{8}$$

Here, k_b is the Boltzmann's constant, T is the ambient temperature, and e_q and e_p^* are the energies of the electron at Q^- (state P^+Q^-) and in the excited state P^*. The difference of these energies depends on the electric field, when this exists. The probability that an electron resides either in the excited state P^*, Q^-, or in the ground state of P [denoted, respectively, by $p(P^*)$, $p(P^+Q^-)$, and $p(P)$], from Fig. 15 are represented by

$$p\left(P^+Q^-\right) = \exp\left(\frac{\Delta\mu - \Delta E}{k_b T}\right) \tag{9}$$

$$p\left(P^*\right) = \frac{K}{k_{cs}} + \exp\left(\frac{\Delta\mu - \Delta E}{k_b T}\right). \tag{10}$$

The rate of change of the electron between the states based on the probability of the electron states is represented by

$$\frac{1}{\tau} p\left(P^*\right) = g + \frac{1}{\tau}\exp\left(\frac{-\Delta E}{k_b T}\right) - K. \tag{11}$$

Substituting (9) and (10) into (11) gives

$$K = K_L - K_O\left(e^{\Delta\mu/k_b T} - 1\right). \tag{12}$$

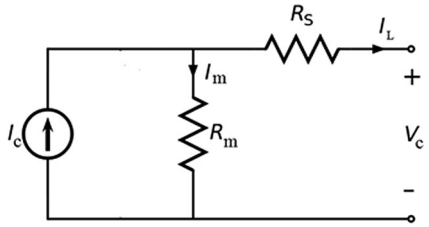

Fig. 16. Electrical equivalent circuit model of electron transport during photosynthesis.

As is clear, (12) is analogous to the Shockley solar cell equation. The reaction rates, K_L and K_O, which correspond to the light and dark reactions, respectively, are given by

$$K_L = \frac{\tau k_{cs}}{1+\tau k_{cs}} g \qquad K_o = \frac{\tau k_{cs}}{1+\tau k_{cs}} e^{-\Delta E/k_b T}. \quad (13)$$

Thus, it is established that photosynthetic reaction models are similar to that of a solar cell. Hence, the electrical equivalent circuit model of the fabricated cell can be developed based on that of a solar cell. As was observed earlier, the V/I relationship is linear. Moreover, there exists an absence of a diode-like behavior (diode voltage and current) in the case of the μPSC. Thus, the diode from the electrical equivalent circuit model of the solar cell can be omitted. Thus, the overall model circuit would be as represented in Fig. 16.

The cell is represented using a current source (I_c—cell current), in parallel with a resistance R_m, which is the resistance of the PEM (the value is typically very high). Obviously, under ideal conditions, R_m should equal to infinity. However, under practical operating conditions, PEM do leak some electrons through it. The cell current, I_c, shown in the equivalent circuit model, flowing through R_m, represents the voltage potential developed across the membrane. The series resistance R_s represents the total series resistance experienced by the load current. The total resistance R_s consists of the resistance of the anode, resistance of the cathode, as well as the resistance of the solution. Apart from the resistances, the cell also exhibits capacitive behavior. This is due to the fact that the PEM is a dielectric by nature. Moreover, the PEM is also sandwiched between two electrodes [17]. This capacitance is predictable and is dependent on the dielectric constants of the PEM, as well as the area of the gold electrode (C_m, as shown in Fig. 17).

The value of C_m typically ranges between 1 and 10 μF. Apart from the capacitance in the PEM, the cell should theoretically have a huge capacitance value at its end terminals, to emulate the large time constant of the system (C_c). However, calculating this time constant and its respective capacitance value for the electrical equivalent circuit is very complex, and has been ignored in this paper. The value is kept significantly low, for simplicity, and it does not affect the voltage and cell current produced. However, this is the only way the cell reacts to changes in load as well as switching commands. Thus, the distinctive electrical equivalent circuit cell model, used for testing and emulation, is shown in Fig. 17.

As addressed earlier, the source is represented using a current source, in parallel with the resistance of the PEM R_m. Also,

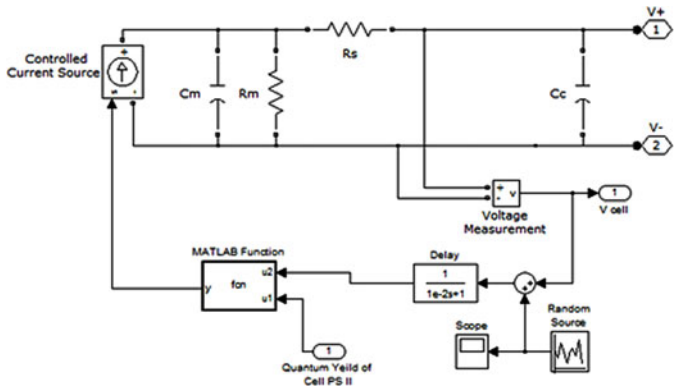

Fig. 17. Electrical equivalent circuit representation of the developed μPSC.

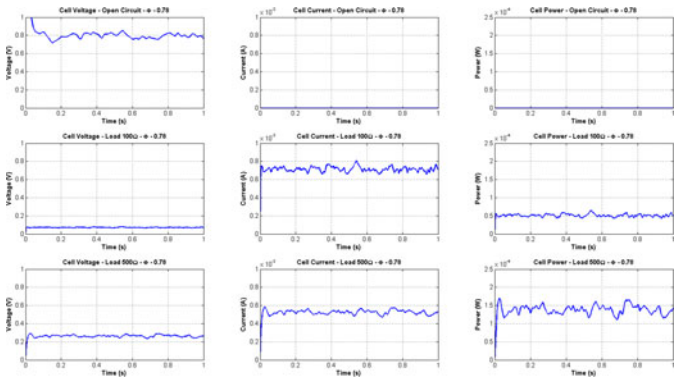

Fig. 18. Emulation test results of equivalent circuit model of μPSC (Φ = 0.78).

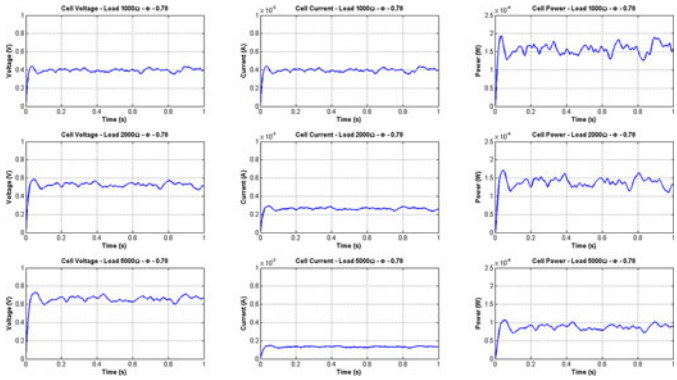

Fig. 19. Emulation test results of equivalent circuit model of μPSC (Φ = 0.78).

C_m represents the membrane's capacitive behavior, and it is connected to the series resistance, R_s. When the cell is under open circuit, there is zero current flowing through the load, and hence, the current flows only through R_m, producing the OCV. The MATLAB function block is used to relate the quantum yield and the voltage produced to estimate the cell current. There is a small delay included for avoiding the algebraic loop error during emulation. The random source represents the minor perturbations that the cell continually produces around an average value. Using this developed electrical model, the cell's behavior for various loads is successfully emulated. Figs. 18 and 19 show

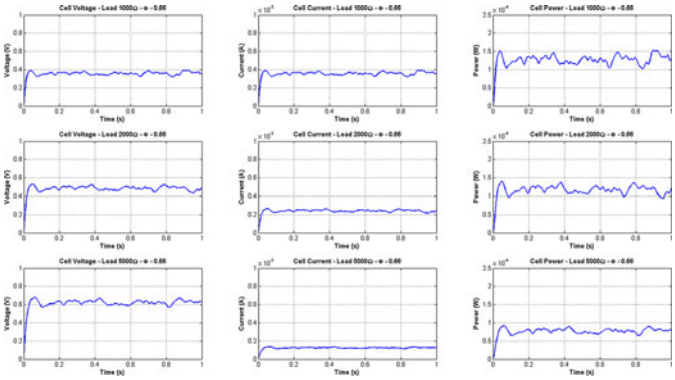

Fig. 20. Emulation test results of equivalent circuit model of μPSC ($\Phi = 0.66$).

TABLE II

	Parameter	QUANTITY	DESCRIPTION
R_m	Resistance of PEM	10k - 1M Ω	Based on Nafion type and water content
C_m	Capacitance of PEM	1μF to 10μF	Based on Nafion type and water content
R_s	Series Resistance	1 - 3 Ω	Resistance of electrodes and leads
C_c	Time constant of system	1 F to few F	1 F gives a rise time of 0.3s

the test results for open circuit, 100 Ω, and 200 Ω loads, as well as for 1000, 2000, and 5000 Ω loads, respectively, for a cell with quantum yield $\Phi = 0.78$. Fig. 20 shows the test results for a cell with $\Phi = 0.66$ and with loads of 1000, 2000, and 5000 ω. Table II shows the values used for the simulation of the equivalent circuit models.

The values mostly used for the simulations were 1 MΩ for R_m and 10 μF for C_m, Nafion 117 was degasified to remove the moisture and used. Series resistance of 1 Ω was used for nonstacks and 2–3 Ω were used, depending on the stack size. The rise time was kept lower than the actual experimental value in order for the simulation to be fast, thus 0.1 F was used for C_c (other values were also used depending upon various conditions as explained earlier).

From the results, it is evident that the cell characteristics are matched by the emulation tests. Furthermore, the test results can be used to study the behavior of the cell, as to how it responds to varying loading conditions. A single μPSC would not suffice to generate adequate amount of energy that can be harvested. In order to harvest significant amount of energy the cells have to be stacked, by connecting them in series and/or parallel, to increase the energy and/or power output. It was proven that stacking of MFCs and μPSCs scales the power produced (Aelterman *et al.*, 2006). In their work, a six-cell stacked configuration was used in series/parallel, and it was concluded that any desired current or voltage could be obtained by combining the appropriate number of series and parallel-connected cells. It was reported that the cell OCV and SCC scaled approximately by factor of 6.0 higher than that of the OCV or SCC of the individual cells [18], [19].

In order to compare the emulation test results of the stacked μPSCs, two sets of experiments were performed, by stacking two individual cells. In the first experiment, two μPSC were connected in series, and in the second one, the same two μPSCs were connected in parallel. Typically, when two similar sources are connected in series, the total voltage will be the sum of the voltages of the individual cells, and the same is true for the current, when similar sources connected in parallel. The experimental results are shown in Figs. 21 and 22. The results are promising, and it can be concluded that the cells are appropriately scalable by stacking them. When connected in series, the voltage scaled by a factor of approximately 2.07, and when connected in parallel, the cell current scaled by a factor of approximately 1.77. It should be noted that the stack has more power density, when stacked in series, compared to the parallel configuration.

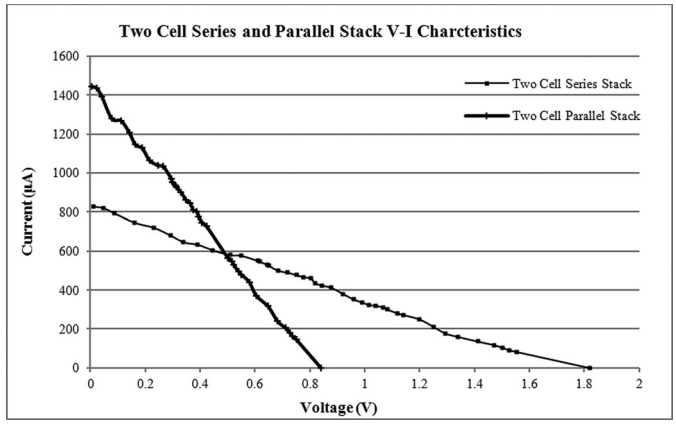

Fig. 21. V/I characteristics of 2-cell series and parallel stack.

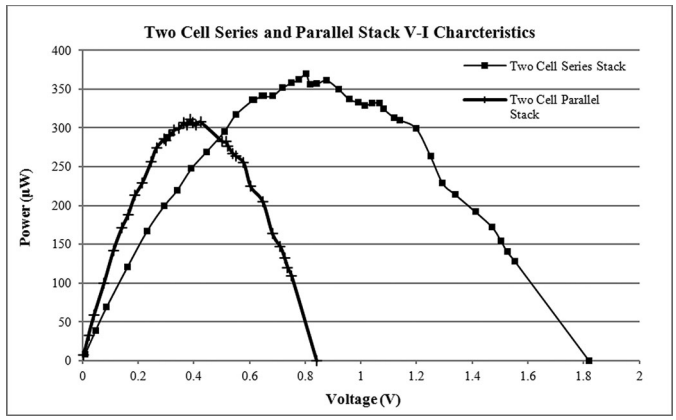

Fig. 22. Power characteristics of 2-cell series and parallel stack.

However, to include accurate scaling factors in emulation tests is an extremely complex process, and further investigations need to be performed, in order to understand, as to how the cell parameters precisely scale. Thus, for simplicity purposes, the cells are directly scaled in the emulation tests. The simulation test results for two cells stacked in series and parallel are shown in Fig. 23 and are compared with the experimental results.

The μPSC equivalent circuit cell model can be stacked in the required configuration and tested. The results will greatly aid further analyses and can be further used to design, simulate, and analyze a suitable power electronic converter, for energy harvesting applications. With the help of the model, using stacked

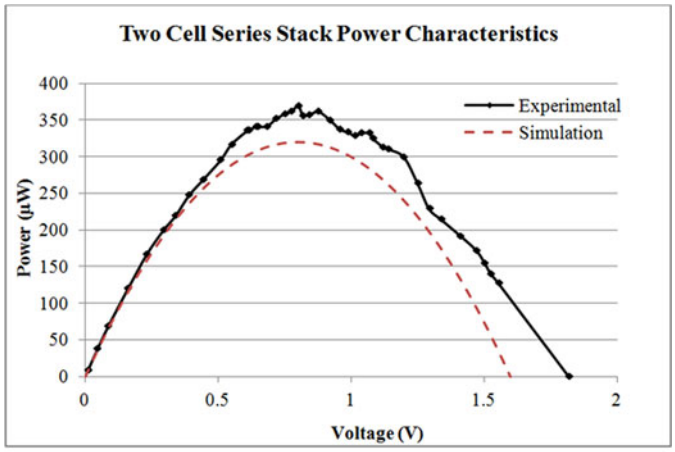

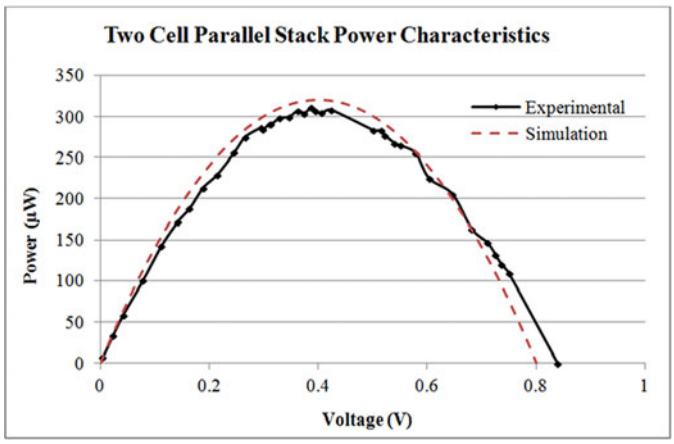

Fig. 23. Comparison of experimental and simulated cell stack results.

μPSC as source, a suitable power electronic energy harvester can be designed and developed to charge a battery.

A 6 × 6 cell stack (6 series × 6 parallel = 36 cells) is used for the simulations. The stack provides 2.4 V at peak power point. A dc–dc synchronous boost converter was designed and simulated for a Li-ion battery charging for the energy harvesting application. A single cell Li-ion with a nominal voltage of 3.7 V and 1.5 mA·h capacity was selected for the application. The dc–dc boost converter was linearized for an output voltage of 4.8 V and operates at MPP, which is the most ideal for Li-ion battery charging applications. The 6S6P stack produces a peak power of 5.8 mW, thus the boost converter operating at output voltage of 4.8 V would deliver a peak current of 1.2 mA. The parameters and topology of the synchronous boost converter are provided in Table III and Fig. 24.

Miniaturized inductors have helped the development of inductor-based converters for energy harvesting applications [20]. The dc–dc boostconverter is widely used in manyenergy harvesting applications [21]–[24]. Along with these, various novel and custom MPPT techniques have been developed for different energy harvesting applications without causing any overhead on operation with the system [25]–[27], which can used as a base for development of a novel and custom MPPT for energy harvesting using PSC (Figs. 25 and 26).

TABLE III

Parameters	QUANTITY
Input Voltage range	1.8 to 3.6 V
Input Power	5.8 mW
Output Voltage	4.8 V
L-Inductance	25 mH
C-Output Capacitor	800 nF
Switching frequency	100 kHz
MOSFET Rds on	360 µΩ
Battery	Li-Ion
Battery Nominal Voltage	3.7 V
Battery Charging Voltage	4.8 V
Battery capacity	1.5 mAh

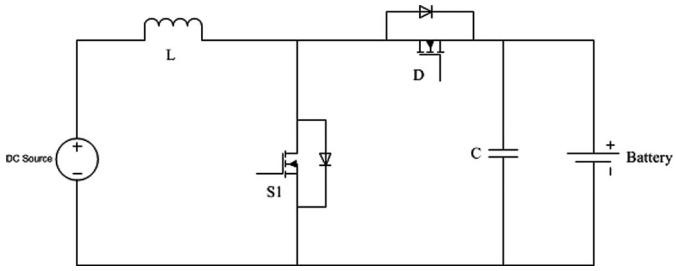

Fig. 24. Synchronous dc–dc boost converter (changed load to battery).

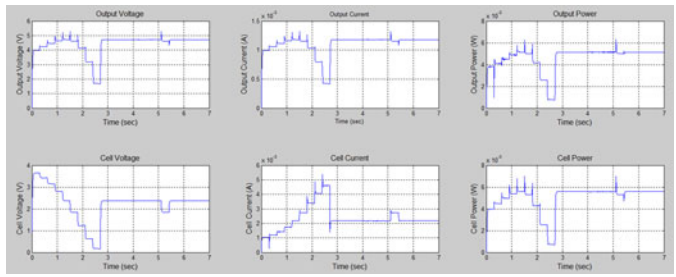

Fig. 25. Boost converter output and 6 × 6 cell stack power output results.

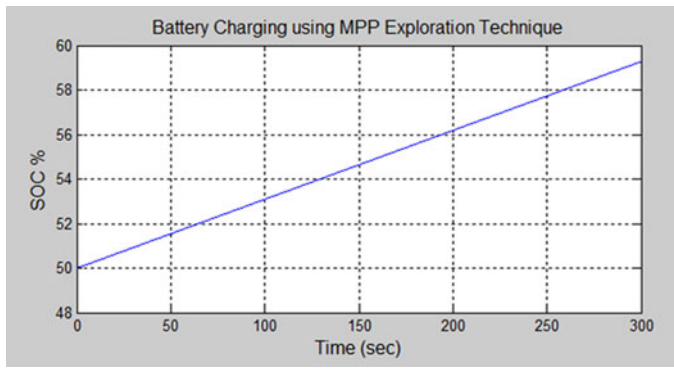

Fig. 26. State of charge of Li-ion battery charged by the boost converter.

It is most advantageous to operate at the MPP. The converter is operated at different duty cycles initially, the duty cycle at which the converter produces the maximum power is selected as the operating duty cycle. This MPPT is being referred as the MPPT exploration technique. The converter is operated with a duty cycle of 0.1 and is incremented by 0.1 until 0.9. The

converter is made to operate for 0.3 s at steady state at each step and the average steady-state power is computed. The converter is then made to operate at the duty cycle at which it produced the maximum power. The converter provides an output of 5 mW with the peak input of 5.8 mW, which translates to 86.2% efficiency where the ESR of the inductor and capacitor are 0.3 and 0.1 Ω, respectively.

V. Conclusion

This paper proposes an electrical equivalent model for a μPSC, which is tested and authenticated with experimental verification on a fabricated prototype. The developed model is further used for testing emulation behavior, to efficiently and accurately design an energy harvesting power electronic converter. The principle of the operation of the device is based on "photosynthesis." The developed model can also be used effectively to design a novel MPP tracking-based energy harvesting converter for the μPSC application. Furthermore, the model can be easily modified to match other MFC characteristics and help build suitable harvesting power converters. Such an integrated cell fabrication approach would enhance the research ecosystem of MFCs and PSCs, and would pave way for the technology and research. This will lead to much improved and sophisticated model development as well as accurate cell behavior emulation methodologies. Such improved models will enable designing and building highly efficient and optimal power electronic converters for MFCs and PSCs.

Through the work presented in this paper, it was also proven that the fabricated μPSCs are easily scalable. This attractive feature promises an exciting prospect of developing larger, more configurable cell stacks, which, in turn, will be able to generate much superior power levels. Thus, moving forward, a strong conclusive case can be made for the maturity of PSCs, in general, which can lead to the development of a fairly cheap and sustainable energy resource.

References

[1] K. B. Lam, E. Johnson, and L. Lin, "A bio-solar cell powered by subcellular plant photosystems," in *Proc. IEEE Int. Conf. Micro Electro. Mech. Syst.*, Maastricht, The Netherlands, Jan. 2004, pp. 220–223.

[2] M. Chiao, K. B. Lam, and L. Lin, "Micromachined microbial and photosynthetic fuel cells," *J. Micromech. Microeng.*, vol. 16, no. 12, p. 2547, Oct. 2006.

[3] D. P. B. T. B. Strik, R. A. Timmers, M. Helder, K. J. J. Steinbusch, H. V. M. Hamelers, and C. J. N. Buisman, "Microbial solar cells: Applying photosynthetic and electrochemically active organisms," *Trends Biotechnol.*, vol. 29, no. 1, pp. 41–49, Jan. 2011.

[4] T. Yagishita, S. Sawayama, K. Tsukahara, and T. Ogi, "Photosynthetic bio-fuel cell using cyanobacteria," *Renewable Energy*, vol. 9, no. 1–4, pp. 958–961, Sep./Dec. 1996.

[5] K. B. Lam, E. A. Johnson, M. Chiao, and L. Lin, "A MEMS photosynthetic electrochemical cell powered by subcellular plant photosystems," *J. Microelectromech. Syst.*, vol. 15, no. 5, pp. 1243–1250, Oct. 2006.

[6] L. Taiz and E. Zeiger, *Plant Physiology*, 5th ed.: Sinauer Associates, May 2010.

[7] S. B. Ku, G. E. Edwards, and C. B. Tanner, "Effects of light, carbon dioxide, and temperature on photosynthesis, oxygen inhibition of photosynthesis, and transpiration in solanum tuberosum," *Plant Physiol.*, vol. 59, no. 5, pp. 868–872, May 1977.

[8] G. Rechtsteiner and J. Ganske, "Using natural and artificial light sources to illustrate quantum mechanical concepts," *Chem. Educator*, vol. 3, no. 4, pp. 1–12, 1998.

[9] "Rate of photosynthesis: Limiting factors," *RSC-Advancing Chemical Sci.*, Oct. 2012.

[10] J. Kobza, E. G. Uribe, and G. J. Williams III, "Temperature dependence of photosynthesis in Agropyron smithii Rydb. III. Responses of protoplasts and intact chloroplasts," *Plant Physiol.*, vol. 75, no. 2, pp. 378–381, Jun. 1984.

[11] S. H. Jin and X. Q. Li, "Effect of elevated air temperature on photosynthesis in a subtropical forest tree, Ficus Concinna," in *Proc. IEEE Int. Conf. Bioinformatics Biomed. Eng.*, Wuhan, China, May 2011, pp. 1–3.

[12] A. Meehan, H. Gao, and Z. Lewandowski, "Energy harvesting with microbial fuel cell and power management system," *IEEE Trans. Power Electron.*, vol. 26, no. 1, pp. 176–181, Jan. 2011.

[13] J. D. Park and Z. Ren, "Hysteresis-controller-based energy harvesting scheme for microbial fuel cells with parallel operation capability," *IEEE Trans. Energy Convers.*, vol. 27, no. 3, pp. 715–724, Sep. 2012.

[14] A. Chaudhary and C. R. Ozansoy, "Microbial electrolysis cell modelling and simulation using MATLAB," in *Proc. IEEE Australasian Universities Power Eng. Conf.*, Adelaide, SA, Australia, Sep. 2009, pp. 1–6.

[15] N. Degrenne, F. Buret, F. Morel, S. Adami, D. Labrousse, B. Allard, and A. Zaoui, "Self-starting dc/dc boost converter for low-power and low-voltage microbial electric generators," in *Proc. IEEE Energy Convers. Congr. Expo.*, Phoenix, AZ, Sep. 2011, pp. 889–896.

[16] T. Markvart and P. T. Landsberg, "Solar cell model for electron transport in photosynthesis," in *Proc. IEEE Photovoltaic Spec. Conf.*, New Orleans, LA, May 2002, pp. 1348–1351.

[17] W. Friede, S. Rael, and B. Davat, "Mathematical model and characterization of the transient behavior of a PEM fuel cell," *IEEE Trans. Power Electron.*, vol. 19, no. 5, pp. 1234–1241, Sep. 2004.

[18] C. Fernández, P. Zumel, V. Valdivia, A. Fernández-Herrero, M. Sanz, A. Lázaro, and A. Barrado, "Simple model and experimental identification of a fuel-cell-based power supply oriented to system-level analysis," *IEEE Trans. Power Electron.*, vol. 26, no. 7, pp. 1868–1878, Jul. 2011.

[19] S. Malo and R. Grino, "Design, construction, and control of a stand-alone energy-conditioning system for PEM-type fuel cells," *IEEE Trans. Power Electron.*, vol. 25, no. 10, pp. 2496–2506, Oct. 2010.

[20] M. Wang, J. Li, K. D. T. Ngo, and H. Xie. (2011, May). A surface-mountable microfabricated power inductor in silicon for ultracompact power supplies. *IEEE Trans. Power Electron*. [Online]. 26(5), pp. 1310–1315. Available: http://ieeexplore.ieee.org/stamp/stamp.jsp?tp=&arnumber=5443595&isnumber=5899001

[21] A. Meehan, H. Gao, and Z. Lewandowski, "Energy harvesting with microbial fuel cell and power management system," *IEEE Trans. Power Electron.*, vol. 26, no. 1, pp. 176–181, Jan. 2011.

[22] G. D. Szarka, B. H. Stark, and S. G. Burrow, "Review of power conditioning for kinetic energy harvesting systems," *IEEE Trans. on Power Electron.*, vol. 27, no. 2, pp. 803–815, Feb. 2012.

[23] G. D. Szarka, S. G. Burrow, and B. H. Stark, "Ultralow power, fully autonomous boost rectifier for electromagnetic energy harvesters," *IEEE Trans. Power Electron.*, vol. 28, no. 7, pp. 3353–3362, Jul. 2013.

[24] I. Laird and D. D. Lu, "High step-up DC/DC topology and MPPT algorithm for use with a thermoelectric generator," *IEEE Trans. Power Electron.*, vol. 28, no. 7, pp. 3147–3157, Jul. 2013.

[25] H. Kim, S. Kim, C.-K. Kwon, Y.-J. Min, C. Kim, and S.-W. Kim, "An energy-efficient fast maximum power point tracking circuit in an 800-μW photovoltaic energy harvester," *IEEE Trans. Power Electron.*, vol. 28, no. 6, pp. 2927–2935, Jun. 2013.

[26] R. Enne, M. Nikolic, and H. Zimmermann, "Dynamic integrated MPP tracker in 0.35 μm CMOS," *IEEE Trans. Power Electron.*, vol. 28, no. 6, pp. 2886–2894, Jun. 2013.

[27] J. Kim and C. Kim, "A DC–DC boost converter with variation-tolerant MPPT technique and efficient ZCS circuit for thermoelectric energy harvesting applications," *IEEE Trans. Power Electron.*, vol. 28, no. 8, pp. 3827–3833, Aug. 2013.

Authors' photographs and biographies not available at the time of publication.